Chemistry Europe
European Chemical Societies Publishing

Synthesis and Properties of Partially Saturated Fluorenyl-Derived [*n*]Helicenes Featuring an Overcrowded Alkene

Lenka Pallova,[a] Etienne S. Gauthier,[b] Laura Abella,[d] Marion Jean,[c] Nicolas Vanthuyne,[c] Vincent Dorcet,[b] Laure Vendier,[a] Jochen Autschbach,*[d] Jeanne Crassous,*[b] Stéphanie Bastin,*[a] and Vincent César*[a]

Abstract: The straightforward, multigram-scale synthesis of the partially saturated H_6-fluoreno[*n*]helicenes ($n = 5$ or 7) featuring a central, overcrowded alkene is described. The key cyclization step was based on an intramolecular McMurry reaction from the corresponding 1,5-diketones. Chiral stationary phase HPLC analysis and isomer separation indicate that each helicenic compound is constituted of three diastereoisomers at room temperature, i.e. the configurationally stable (*R,R,P*)/(*S,S,M*) pair of enantiomers and an apparently achiral compound resulting from the rapid interconversion between the (*R,S,P*) and (*S,R,M*) enantiomers. The partially saturated H_6-fluoreno[*n*]helicenes are oxidatively aromatized to give an efficient access to the corresponding fluoreno[*n*]helicenes. The chiroptical properties (vibrational and electronic circular dichroism) of the chiral, enantiopure compounds have been measured and analyzed by quantum-chemical calculations, confirming their helicoidal nature.

Introduction

Helicenes are a special class of inherently chiral molecules that combine a helical topology and an extended π-conjugated structure.[1] Owing to this unique screw-shaped π-delocalization, helicenes display enhanced chiroptical properties (Optical Rotation (OR), Electronic Circular Dichroism (ECD), Circularly Polarized Luminescence (CPL) …) compared to other common chiral molecules.[1,2] Thus, they have gained great significance over the past decade as key constitutional units in materials for optoelectronics,[3,4] supramolecular chemistry,[5] chiroptical switches[6] or in the design of chiral ligands for asymmetric catalysis to name a few.[1f,7] At the heart of these blossoming applications lies the possibility to tune the chiroptical properties of helicenic compounds by modifying their structure. Starting from the basic carbo[*n*]helicenes, formally composed of *ortho*-fused benzene rings, several strategies were indeed found suitable to increase the diversity of helicenic scaffolds by: *i*) introducing main-group elements (B, Si, N, P …) leading to the design of heterohelicenes;[8] *ii*) varying the size and nature of the rings within the helix; *iii*) designing helicenoid or helicene-like systems formed of non-fully aromatic *ortho*-fused rings;[9] *iv*) inclusion of a positive or negative charge within the helical scaffold,[10] or *v*) incorporating helicenic ligands into organometallic complexes.[11] In this context, the development of efficient, flexible and convenient methods for the synthesis of helicenic compounds appears of utmost importance, as the field cannot grow without the advent of more practical, scalable and cost-efficient synthetic pathways.

In a joint research program, we were interested in using the [5] and [7]-helicene-like fluorenes **1** and **2** as building blocks to generate novel helicene-NHC-based ligands for organometallic chemistry (Figure 1).[12,13] While the dibenzo[*c,g*]fluorene **1** (dbf) has been known for more than half a century,[14] the [7] helicene-like fluorene **2** was described in 2016 by Nozaki.[15,16] Both compounds are obtained by reduction of the corresponding ketone analogues using hydrazine at elevated temperature. Moreover, the syntheses of the keto-compounds involve either a decarboxylative condensation of binaphthyl 2,2′-dicarboxylic acid under very harsh conditions (300 °C) or a transition-metal catalyzed, multistep synthesis. We thus devised to develop a common, direct and efficient synthetic protocol towards the fluoreno[*n*]helicenes **1** and **2** from easily available starting materials and without going through the ketone intermediates. Our strategy relies on the key intermediates **3** and **4**, which would generate compounds **1** and **2** respectively in a final dehydrogenative aromatization. Compounds **3** and **4** are thus partially hydrogenated (or saturated) fluoreno[*n*]helicenes, and their most striking feature is the presence of a *tetra*-substituted,

[a] *Dr. L. Pallova, Dr. L. Vendier, Dr. S. Bastin, Dr. V. César*
LCC-CNRS
Université de Toulouse, CNRS, 31077 Toulouse (France)
E-mail: stephanie.bastin@lcc-toulouse.fr
vincent.cesar@lcc-toulouse.fr

[b] *Dr. E. S. Gauthier, Dr. V. Dorcet, Dr. J. Crassous*
Institut des Sciences Chimiques de Rennes, UMR 6226
Institut de Physique de Rennes, UMR 6251, Campus de Beaulieu
CNRS-Université de Rennes 1, 35042 Rennes Cedex (France)
E-mail: jeanne.crassous@univ-rennes1.fr

[c] *M. Jean, Dr. N. Vanthuyne*
Aix Marseille university, CNRS, Centrale Marseille, Ism2
13397 Marseille (France)

[d] *Dr. L. Abella, Prof. J. Autschbach*
Department of chemistry, University at Buffalo – State University of New York
Buffalo, NY 14260 (USA)
E-mail: jochena@buffalo.edu

Supporting information for this article is available on the WWW under https://doi.org/10.1002/chem.202100150

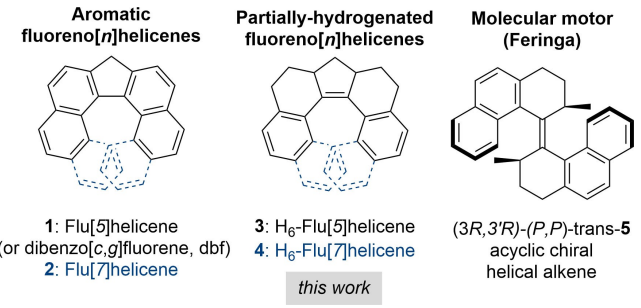

Figure 1. Structures of helicene-like fluorenes **1** and **2**, of their partially hydrogenated analogues **3** and **4** and of the related acyclic, overcrowded alkene **5**. Notation: Compounds **1** and **3** are composed of the five *ortho*-fused rings in black, while compounds **2** and **4** (in blue) possess the five rings in black and the two additional terminal phenyl rings in blue.

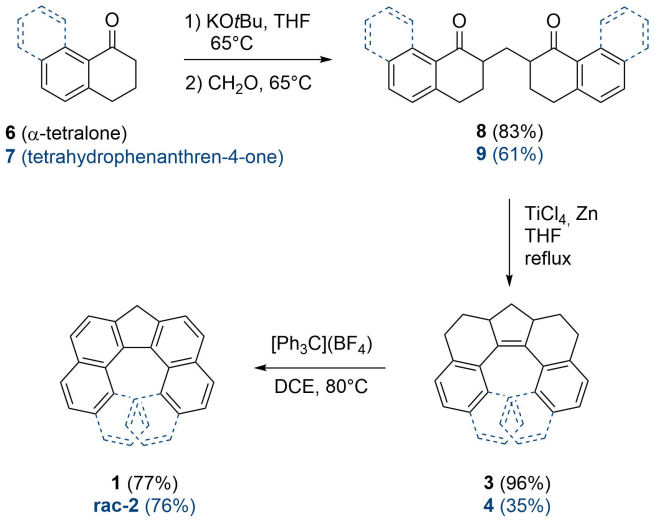

Scheme 1. Optimized synthetic route to the fluoreno[*n*]helicenes **1** and **2**.

overcrowded C=C bond. As such, they can be considered as the cyclic analogues of the chiral helical alkene (3*R*,3′*R*)-(*P*,*P*)-*trans*-**5**,[17] which is the archetype of the well-known Feringa's molecular motors.[18]

We report herein the efficient, multi-gram scale synthesis of compounds **3** and **4**, along with the isomer separation, structural characterization of their different stereoisomers. The solution behavior and chiroptical properties of the latter have been examined and analyzed with the help of quantum-chemical calculations, as well as their conversion into the aromatic Flu[*n*]helicenes.

Results and Discussion

Synthesis and characterization of the partially saturated fluoreno[*n*]helicenes 3 and 4 and of the aromatic fluoreno[*n*] helicenes 1 and 2 (*n* = 5, 7)

By analogy to the synthesis of the acyclic chiral helical alkene (3*R*,3′*R*)-(*P*,*P*)-*trans*-**5**, the key final cyclization step leading to **3** and **4** was devised through a McMurry coupling reaction between the two carbonyl moieties of the corresponding symmetrical 1,5-diketones **8** and **9** respectively. By optimizing the direct, base-assisted condensation of formaldehyde with 2 equivalents of α-tetralone **6** or tetrahydrophenanthren-4-one **7**,[19,20] the synthesis of the 1,5-diketones **8** and **9** was found to proceed efficiently in good yields and on a multi-gram scale (up to 18 g) (Scheme 1). Compounds **8** and **9** are each composed of an equimolar mixture of the racemic (*R*,*R*)/(*S*,*S*) couple and of the (*R*,*S*) meso compound.

Then, submitting the 1,5-diketone **8** to the McMurry conditions cleanly furnished the corresponding partially saturated helicene-like compound **3** in an excellent 96% isolated yield after column chromatography (Scheme 1). While its formulation was firmly inferred from HRMS and elemental analysis, the ^{1}H NMR spectrum of **3** after chromatography indicated the presence of 2 diastereoisomers at room temperature in a ratio 2.3/1, which was further confirmed by HPLC (*vide infra*). Gratifyingly, the [7]-helicene-like alkene **4** was also obtained under the same conditions from **9**, albeit in a lower yield of 35%, which can be ascribed to the high steric congestion around the generated, internal C=C double bond. Analogously to compound **3**, the analysis of the ^{1}H NMR spectrum of **4** recorded at room temperature led to the conclusion that **4** might be composed of a diastereoisomeric mixture (ratio of 1.77/1), whose one diastereoisomer exhibits a fluxional process in view of the broad signals observed for one set of the signals (*vide infra*).[20] Noteworthy, both reactions could be carried out on a multi-gram scale, which is highly beneficial to the synthetic utility of the strategy.

The last aromatization step was performed directly on the diastereoisomeric mixtures of the partially saturated **3** and **4** without further separation of the latter and consists in an oxidative dehydrogenation using tritylium tetrafluoroborate as hydride scavenger. The aromatic helicenic fluorenes **1** and **2** were smoothly isolated in 77% and 76% yields, respectively. While the dibenzo[*c*,*g*]fluorene **1** is not configurationally stable and is thus achiral, the [7]-helicene-like fluorene **2** was obtained as a racemic mixture and the *M* and *P* enantiomers of **2** were obtained with ee values of more than 99.5% and 98.5% respectively by preparative HPLC separation on a chiral stationary phase, following the conditions reported by Nozaki.[15a]

Isomer separation of the stereoisomers of 3 and 4, their structural characterization and their solution behavior

The H_6-Flu[*n*]helicenes **3** and **4** possess two stereogenic carbon atoms at the bridgeheads between the cyclopentenyl and the neighboring cyclohexenyl rings, and – *a priori* - a helical chirality, which led to consider the possible generation of the three pairs of enantiomers depicted in Scheme 2. The two pairs of C_2-symmetric enantiomers (*R*,*R*,*P*)/(*S*,*S*,*M*) and (*R*,*R*,*M*)/(*S*,*S*,*P*) share the same central chirality and only differ by their helicity,

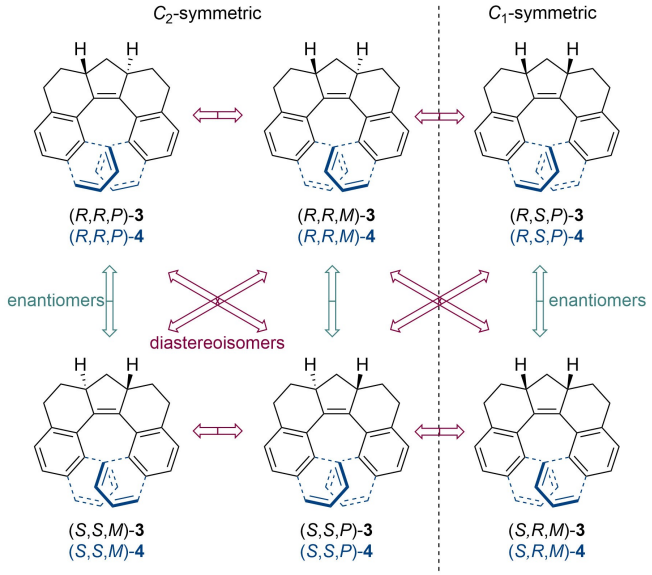

Scheme 2. General depiction of the possible stereoisomers for compounds **3** and **4** and the respective relationships between them.

and thus should be energetically different. On another hand, each enantiomer of the (*R,S,P*)/(*S,R,M*) couple is C_1-symmetric.

The HPLC analysis of the crude stereoisomeric mixture of **3** on a chiral stationary phase showed three peaks and the chiral resolution of **3** by HPLC on a preparative scale enabled the isolation of the corresponding three diastereoisomers of **3**. While the second eluted compound is achiral, the first and third eluted compounds correspond to a pair of enantiomers, as confirmed by their mirror-image spectra of electronic circular dichroism (ECD) (see Figure 6a), and were isolated in remarkable >99.5% optical purities. Noteworthy, the ratio between the isolated diastereoisomers of 2.4/1 is consistent with the ratio measured by ^{1}H NMR on the mixture of **3** before the chiral resolution (2.3/1). The ^{1}H NMR spectrum of the achiral diastereoisomer features a diastereotopic pattern for the apical CH_2 protons of the cyclopentenyl ring, with one resonating at $\delta = 2.35$ ppm (dt, $J = 11.8$, 6.1 Hz) and the other one at $\delta = 1.22$ ppm (pseudo-q, $J = 11.1$ Hz). It is also consistent with a C_s-symmetry of the molecule. Indeed, considering that (*R,S,P*)/(*S,R,M*)-**3** is a chiral C_1-symmetric molecule, of overall apparent C_s symmetry in NMR due to unstable helical configuration, the achiral diastereoisomer could be firmly assigned to the enantiomers (*R,S,P*)/(*S,R,M*)-**3**, which are in fast equilibrium at room temperature. Moreover, decreasing the temperature up to −80 °C did not allow to freeze this interconversion process and the achiral compound was then best described as the *meso* compound (*R,S*)-**3**. As expected, the ^{1}H NMR spectrum of the isolated pair of enantiomers confirmed their C_2-symmetry, with a triplet at $\delta = 1.87$ ppm ($J = 7.1$ Hz) corresponding to the two equivalent, apical CH_2 protons. At that point, the helical configuration could not be determined yet and we decided to perform DFT calculations using Gaussian 16,[21] the B3LYP functional,[22] the def2-SV(P) basis set for atoms,[23] and the polarizable continuum model (PCM) for dichloromethane.[24]

The DFT-optimized structures for the different stereoisomers and the calculations of their relative energies revealed that the enantiomers (*R,R,P*)-**3** and (*S,S,M*)-**3** are just 0.4 kcal.mol^{-1} higher in energy than the achiral meso compound (*R,S*)-**3** (Table 1). However, the energy level of 7.8 kcal.mol^{-1} (relative to (*R,S*)-**3**) of the diastereomeric compounds (*R,R,M*)-**3** and (*S,S,P*)-**3** is too high to allow the existence to these compounds, and confirms that only the pair of enantiomers (*R,R,P*)-**3** and (*S,S,M*)-**3** and the achiral, "meso" compound (*R,S*)-**3** are observed experimentally. This analysis also revealed that, despite having only 5 ortho-fused cycles, (*R,R,P*)-**3** and (*S,S,M*)-**3**, are configurationally stable and that the helical chirality is dictated by the central chirality of the two carbon atoms. Moreover, a conformational search on the diastereoisomers yielded two conformers for each compound, which differ in the ring puckering of the cyclohexenyl rings adjacent to the central cyclopentenyl ring (see Supporting Information for details).

Similar chiral stationary phase HPLC analysis and resolution were performed on compound **4** and showed that the diastereoisomeric mixture of **4** is also composed of a pair of enantiomers as first and third eluted compounds and of an ECD-non-responsive compound as the second eluted compound. Concerning the pair of enantiomers, their NMR spectra are consistent with a C_2-symmetry and present in particular a typical triplet signal at $\delta = 2.17$ ppm ($J = 6.9$ Hz) corresponding to the apical CH_2 protons of the cyclopentenyl ring. Moreover, a first proof of the helical structure was found in the significantly high field-shifted resonance at $\delta = 6.52$ ppm (ddd) of two aryl protons compared to the other aromatic protons, as they experience the aromatic ring current anisotropy generated by the close proximity of the naphthalene moiety in the opposite part of the molecule. To unequivocally prove the molecular geometry and the complete configuration of this pair of enantiomers, single crystals of the first eluted enantiomer suitable for an X-Ray diffraction analysis were grown (Figure 2).[25] The crystal was found to be orthorhombic with the space group $P2_12_12_1$ and it corresponds to (*R,R,P*)-**4** stereoisomer. As it is apparent from Figure 2, the naphthalene moiety and the proton at the stereogenic carbon atom of the same one-half of the molecule are orientated on the same side of the plane defined by C14, C1, C29 and C16. The central double

Table 1. Computed relative energies of stereoisomers of **3** and **4**.[a]

Compound	E_{rel} (kcal.mol^{-1})[b]
(*R,R,P*)-**3**/(*S,S,M*)-**3**	0.4 (conformer 1) 2.2 (conformer 2)
(*R,R,M*)-**3**/(*S,S,P*)-**3**	7.8
(*R,S,P*)-**3**/(*S,R,M*)-**3**	0.0 (conformer 1) 2.6 (conformer 2)
(*R,R,P*)-**4**/(*S,S,M*)-**4**	0.0 (conformer 1) 0.0 (conformer 2)
(*R,R,M*)-**4**/(*S,S,P*)-**4**	13.2
(*R,S,P*)-**4**/(*S,R,M*)-**4**	2.4 (conformer 1) 3.7 (conformer 2) 16.2 (conformer 3)

[a] The different conformers are depicted in the Supporting Information. [b] The energies are given relative to the more stable stereoisomer and conformer.

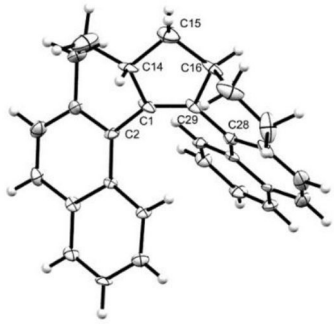

Figure 2. Molecular structure of (*R,R,P*)-**4** determined by XRD analysis (ellipsoids drawn at 30% probability level). Selected bond length: C1–C29 1.352(9) Å.

bond C1–C29 [1.352(9) Å] is only slightly elongated compared to the literature values of 1.323 Å for cyclopentene derivatives,[26] and is highly similar to the other over-crowded C=C bonds reported in related Feringa's molecular motors [1.345–1.350 Å].[17b,27] The sp^2-hydridization of C1 and C29 carbon atoms is evidenced by the sum of the bond angles around them very close to 360° [ΣC1 = 360° and ΣC29 = 359.2°]. The central, over-crowded C1=C29 bond is only slightly twisted [dihedral angles: C14–C1–C29–C28 = 168.65°, C2–C1–C2C16 = 179.45°, C14-C1-C29–C16 = 0.06°, C2–C1–C29–C28 = −11.98°], which is quite similar to the case of the acyclic analogue (3*R*,3'*R*)-(*P,P*)-*trans*-**5**. Eventually, the helicity (dihedral angle between the terminal rings) of (*R,R,P*)-**4** is 56.33°, which is quite similar to the values recorded for [6]-carbohelicene (58.5°),[28] and – more importantly –higher than the value of 42.17° measured for the aromatized Flu[7]helicene **2**.[15a]

The ECD-non responsive second eluted compound exhibits a symmetrical ^{1}H NMR spectrum (recorded at 300 MHz) at 25 °C but the presence of some broad signals suggested a fluxional process. A variable-temperature NMR experiment was thus carried out. Upon lowering the temperature down to −80 °C, all signals became duplicated (Figure S1.13), indicating that the dynamic process was frozen at that temperature and that the molecule is C_1-symmetric, as all protons are unequivalent. This led us to assign this compound as the pair of enantiomers (*R,S,P*)-**4** and (*S,R,M*)-**4**, in which the helical chirality is not configurationally stable at room temperature with a rapid interconversion of the two helixes at that temperature (Scheme 3).

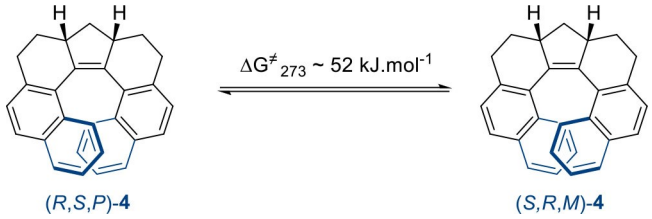

Scheme 3. Interconversion equilibrium between the (*R,S,P*)-**4** and (*S,R,M*)-**4** enantiomers.

The VT NMR behavior of the (*R,S,P*)-**4** and (*S,R,M*)-**4** couple is illustrated in Figure 3 on the more shielded aromatic protons H_a and H_b. In the ^{1}H NMR spectrum recorded at 25 °C on a 600 MHz spectrometer, only one broad signal at $\delta = 6.39$ ppm is observed for the two protons, indicating a fast exchange process at that temperature. At 0 °C, this resonance coalesces, and two signals at $\delta = 6.16$ ppm and 6.58 ppm are detected at –80 °C. The estimated $\Delta G^{\neq}$ of the exchange process associated with this coalescence is ca. 52 kJ.mol^{-1}.

The formulation of this compound as the racemic mixture between (*R,S,P*)-**4** and (*S,R,M*)-**4** was then firmly confirmed by an XRD analysis of single crystals grown at room temperature. It consists of the racemate and crystallizes in the centrosymmetric space group P21/c. The two enantiomers found in the unit cell are depicted in Figure 4. Unfortunately, the poor quality of the crystal prevented any discussion on the metrics and only proved molecular architecture.

DFT calculations (see Computational Details) confirmed the experimental results and showed that the (*R,R,M*)-**4**/(*S,S,P*)-**4** pair is 13.2 kcal.mol^{-1} higher in energy than (*R,R,P*)-**4**/(*S,S,M*)-**4**, which explains why only the latter pair of enantiomers was isolated. It is worth noting that this is the same trend as in the case of the 5-ring-containing compound **3**, where the energy difference is 7.8 kcal.mol^{-1}. The energy difference is higher in **4** due to the presence of the two additional terminal aryl rings. In a conformational search, two iso-energetic conformers for (*R,R,P*)-

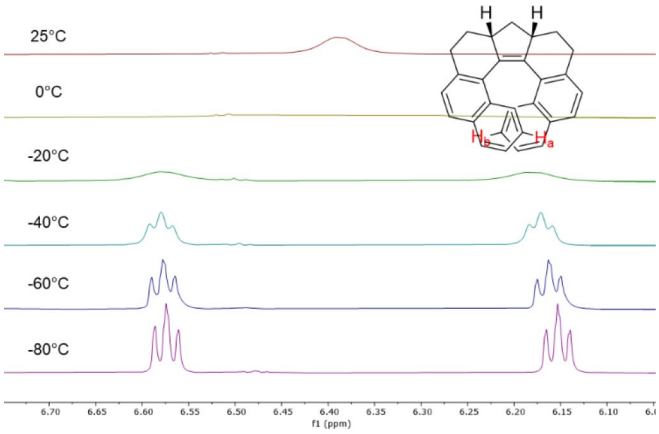

Figure 3. Variable temperature ^{1}H NMR spectra of (*R,S,P*)/(*S,R,M*)-**4** in the region 6.75–6.05 ppm (CD_2Cl_2, 600 MHz).

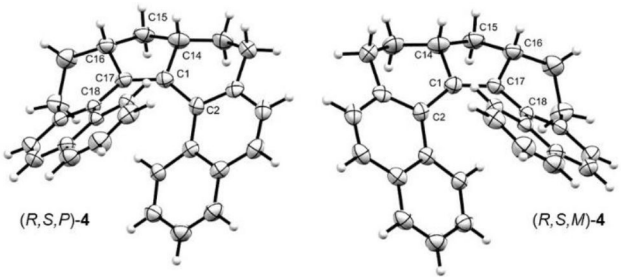

Figure 4. Molecular structure of the racemate (*R,S,P*)-**4** and (*S,R,M*)-**4** determined by XRD analysis (ellipsoids drawn at 30% level of probability).

4/(*S,S,M*)-**4** were identified, which only differ in the ring puckering of the cyclohexenyl rings. The average energy (*R,S,P*)-**4**/(*S,R,M*)-**4** was calculated at 2.4 kcal.mol^{-1} above the most stable (*R,R,P*)-**4**/(*S,S,M*)-**4** stereoisomers and three conformers were identified (Figure S2.2 and S2.3). While the most stable conformer of (*R,S,P*)-**4**/(*S,R,M*)-**4** corresponds to the structure determined by crystallographic analysis, a second possible conformer is only 1.3 kcal.mol^{-1} higher in energy. The high energy of a third conformer at 13.8 kcal.mol^{-1} excludes its presence in the experiments.

VCD spectroscopy

To get more insights into conformational and stereochemical features, these helical crowded alkenes were studied by infrared and vibrational circular dichroism (VCD) spectroscopy.[29] Indeed, helical organic molecules are known to display clear strong VCD signals originating from stretching and bending modes that are generally coupled[30] and that are diagnostic of their absolute stereochemistry obtained by comparison with theory. The experimental IR and VCD spectra of enantiopure compounds **2**, **3** and **4** were measured in CD_2Cl_2 at concentrations around 0.15 M, in the 1000–2000 cm^{-1} region. As depicted on Figures 5a,b and d,e both enantiomers of **3** and **4** display similar IR and mirror-image VCD signatures, with several clear active bands that have been analyzed by theory. Compared to (*R,R,P*)/(*S,S,M*)-**3**, the VCD spectra of (*R,R,P*)/(*S,S,M*)-**4** appear richer and less defined due to the presence of many peaks of moderate intensity.

The calculated VCD spectra for enantiomers (*R,R,P*) and (*S,S,M*) of **3** and **4** are displayed in Figures 5c and 5f. They are Boltzmann-averaged for the two conformers found for (*R,R,P*) and (*S,S,M*) of both compounds. Calculations well reproduce the experiments. Notably, for both **3** and **4**, five dominant peaks are numbered in the VCD spectra, corresponding to the vibrational normal modes shown in Figures S2.8 and S2.10, respectively. For enantiomers (*R,R,P*)-**3** and (*S,S,M*)-**3**, the type of vibrations observed from low to high wavenumber are found as follows: bending at 1287 cm^{-1} (peak 1), combination of bending and stretching at 1393 cm^{-1} (peak 2), stretching at 1510 cm^{-1} (peak 3) and bending at 1524 and 1660 cm^{-1} (peaks 4 and 5, respectively) (see Figures 5c and S2.7 and S2.8). For enantiomers (*R,R,P*)-**4** and (*S,S,M*)-**4**, the assignment corresponds to bending at 1252 cm^{-1} (peak 1), C–C stretching at 1341 cm^{-1} (peak 2), combination of bending and stretching at 1392 cm^{-1} (peak 3) and bending at 1431 and 1500 cm^{-1} (peaks 4 and 5, respectively) (see Figures 5f and S2.9 and S2.10). Finally, comparison between experimental and theoretical VCD enabled to assign the absolute configurations of **3** and **4** (*i.e.* (*R,R,P*)-(+) and (*S,S,M*)-(−), see the Supporting Information part for the specific rotation values).

Analogously to **3** and **4**, (*M*) and (*P*) enantiomers of helicenic fluorene **2** display similar experimental IR and mirror-image VCD spectra (see Figures S2.4 and 2.6). Seven dominant peaks are numbered in the VCD spectra of fluorene **2** (Figures S2.4

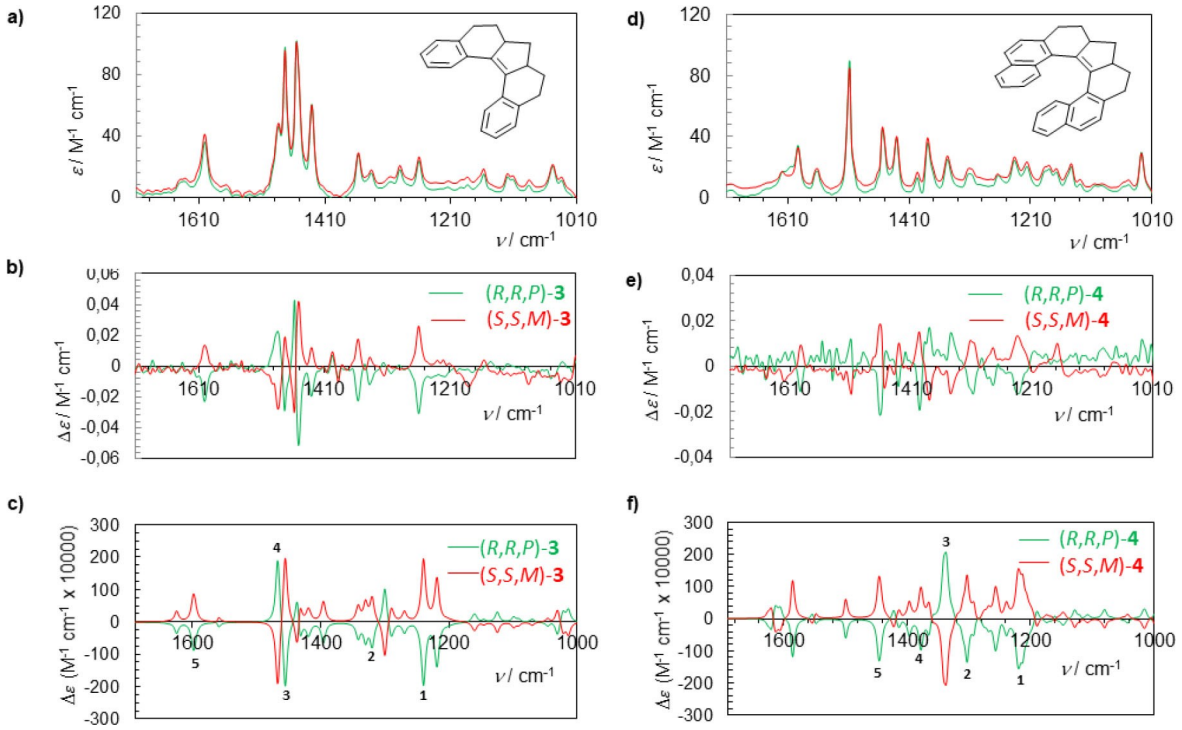

Figure 5. a) Experimental IR and b) VCD spectra of enantiopure (*R,R,P*)-**3** and (*S,S,M*)-**3**. c) Calculated VCD spectra for (*R,R,P*)-**3** and (*S,S,M*)-**3**. The numbers indicate the corresponding peak associated to the vibrational normal modes visualized in Figure S2.8. d) Experimental IR and e) VCD spectra of enantiopure (*R,R,P*)-**4** and (*S,S,M*)-**4**. f) Calculated VCD spectra for (*R,R,P*)-**4** and (*S,S,M*)-**4**. The calculated VCD spectra correspond to the Boltzmann average of the two conformers of (*R,R,P*)-**3** and (*R,R,P*)-**4**. The numbers indicate the corresponding peak associated to the vibrational normal modes visualized in Figure S2.10.

and S2.5). Calculation shows bending vibrations in all the numbered peaks with the only exception of peak 3 at 1342 cm^{-1}, which is a combination of bending and stretching vibrations. Here again, the good agreement between calculation and experiment enabled to assign the (*P*)-(+) and (*M*)-(−) absolute configurations of **2**.

UV-Vis and ECD spectroscopy

Helical molecules display characteristic experimental absorption and electronic circular dichroism (ECD) spectra that can also be used to describe their inherent stereochemistry.[1] UV-vis and ECD spectra of compounds **2**, **3** and **4** were therefore measured (in CH_2Cl_2 at concentrations around $5x10^{-5}$ M) and compared to the calculated ones. The UV-vis spectra are reported in Figures S2.14 and 2.17 while the ECDs are depicted in Figure 6a and c for **3** and **4**, respectively, and in Figure S2.13 for **2**. For instance, the ECD spectrum of (+)-**3** displays a strong positive band at 185 nm ($\Delta\varepsilon = +77\ M^{-1}cm^{-1}$), a strong negative band at 200 nm (-69) followed by a band of moderate intensity at 227 nm (−26) and two strong positive ones at 241 (+39) and 245 (+45) nm, and finally a broad negative band of weak intensity at 290 nm (−7). Calculated spectra determined from time-dependent DFT (TD-DFT) linear response calculations, were performed with the PBE0[31] functional, the def2-SV(P) basis and solvent effects for dichloromethane. Regarding the general performance of TD-DFT for chiroptical spectra, see, for example, references [32a] and [32b]. The calculated UV/Vis spectra for the two conformers found for enantiomers (*R,R,P*)-**3** and (*S,S,M*)-**3** are shown in Figure S2.14. The experimental and the Boltzmann-averaged computational spectra are in good agreement. Three distinct spectral bands can be identified, which are assigned from low to high energy as resulting predominantly from the following occupied-to-unoccupied orbital transitions: HOMO to LUMO, HOMO-1 to LUMO, and HOMO-1 to LUMO+2 (see selected molecular orbitals in Figures 6e and S2.15). The molecular orbitals (MOs) of (*R,R,P*)-**3** associated with the most intense excitations (Table S2.2) are provided in Figure S2.15. For (*R,R,P*)-**3**, the HOMO and the LUMO are localized on the π-conjugated system and the two fragments are involved, while the HOMO-1 is mainly localized on one of the π-conjugated six-membered rings. We note that the HOMO-1 and HOMO-2 levels are quasi-degenerate, with a very small energy difference of 0.067 eV, essentially corresponding to in-phase and out-of-phase (+/−) linear combinations of orbitals on either one of the moieties. The broadened calculated ECD spectra are in very good agreement with the experiments (Figures 6b and 6d and S2.16). The calculated ECD peaks are systematically blue shifted by 0.1–0.3 eV, which is not unusual due to the combination of approximations made in the TD-DFT calculations. In general, the transitions with large oscillator strength *f* also have large rotatory strength *R*, and the assignments of the ECD bands are of course in line with the absorption peaks at wavelengths where both types of spectra have peaks. Additionally, two π→π* electronic transitions appear active in the ECD spectra, from excitation #7 (HOMO-3 to LUMO) and excitation #23 (HOMO-3 to LUMO+3). The latter excitation shows the largest *R* value (415), leading to the strongest band of the ECD spectrum. Finally, comparison

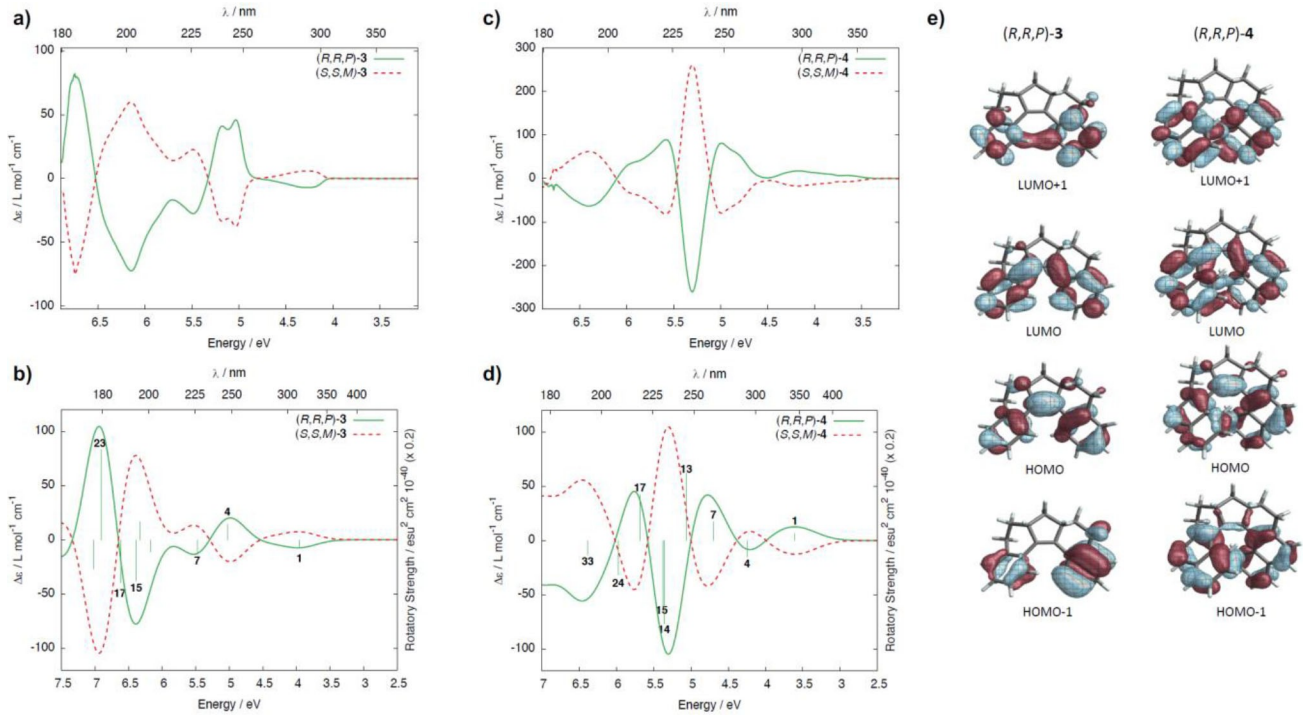

Figure 6. Experimental ECD spectra of a) (*R,R,P*)-**3**/(*S,S,M*)-**3** and c) (*R,R,P*)-**4**/(*S,S,M*)-**4**. Calculated ECD spectra of b) (*R,R,P*)-**3**/(*S,S,M*)-**3** and d) (*R,R,P*)-**4**/(*S,S,M*)-**4**. e) Selected isosurfaces (±0.03 au) of MOs for **3** and **4**.

between experiment and theory enabled to confirm the (*R,R,P*)-(+) and (*S,S,M*)-(−) absolute configurations for **3**.

Two dominant spectral regions with distinct intensities can be identified for the absorption spectra of (*R,R,P*)-**4** and (*S,S,M*)-**4**, which are assigned from low to high energy as resulting predominantly from transitions among the following pairs of occupied and unoccupied MOs: HOMO to LUMO for the low-intensity low-energy region and HOMO-1 to LUMO+2 and LUMO+3 for the high-intensity high-energy region (see Figures S2.17 and S2.18, and Table S2.3). Like in the (*R,R,P*)-**3** system, the highest occupied and lowest unoccupied MOs are localized over the π-conjugated system. We note that the LUMO+2 and LUMO+3 with a small energetic splitting are mainly localized on one moiety, with some contributions from the other moiety, in an in-phase/out-of-phase sign relationship. The ECD spectra of (*R,R,P*)-**4** and (*S,S,M*)-**4** are in line with the absorption spectra, but also showing additional features such as a weak negative band from the HOMO-1 to LUMO+1 transition (exc. #4 at 292 nm) and an intense positive band for HOMO-4 and HOMO-2 to LUMO transitions (exc. #7 at 264 nm). Like in the UV/Vis spectra, the strongest band in the ECD spectra also appear at 230 nm, caused by excitations #14 and #15 with rotatory strengths of −385 and −305 esu^{2}cm^2, respectively. Similarly to **3**, comparison between experiment and theory enabled to confirm the (*R,R,P*)-(+) and (*S,S,M*)-(−) absolute configurations for **4**.

For helicenic fluorene **2**, the calculated UV/Vis spectrum reveals the appearance of four absorption regions with distinct intensities (Figure S2.11). The assignment of the absorption bands from low to high energy is as follows; HOMO to LUMO, HOMO to LUMO+2, HOMO-2 to LUMO+3 and HOMO-2 to LUMO+4. The HOMO and LUMO of (*P*)-**2** are mostly localized on the π-conjugated system of the hexagonal rings close to the pentagon (Figure S2.12). The calculated broadened ECD spectrum of (*P*)-**2** reproduces the experimental spectrum very well (Figure S2.13). Excitation #4 at 317 nm has a particularly large rotatory strength (*R*=648) and corresponds to a combination of two helicene π→π* transitions from HOMO-2 to LUMO and HOMO to LUMO+1. Comparison between experiment and theory enabled to confirm the (*P*)-(+) and (*M*)-(−) absolute configurations for **2**.

Stereoselectivity of the oxidative aromatization of 4 to the fluoreno[*7*]helicene 2

In the first part of this work, the fluoreno[7]helicene **2** was obtained as a racemic mixture from the mixture of stereoisomers of **4**. Having in hand the enantiopure (*R,R,P*)-**4** and its enantiomer (*S,S,M*)-**4**, we were prompted to study the stereoselectivity of the oxidative aromatization reaction under the standard reaction conditions, namely reaction with tritylium tetrafluoroborate in DCE at 80 °C for 3 hours. Starting from the enantiopure (*R,R,P*)-**4** (99.5 % ee) led to the isolation of (*P*)-**2** in 81 % yield but with a diminished ee of 46 % (Scheme 4). A similar drop of enantiopurity was observed with the opposite enantiomer (*S,S,M*)-**4** (99.5 % ee), as it furnished (*M*)-**2** in 71 % and in 42 % ee. These results led to the conclusion that, while the reaction is stereospecific, it is not 100 % stereoselective as an erosion of the enantiopurity was observed.

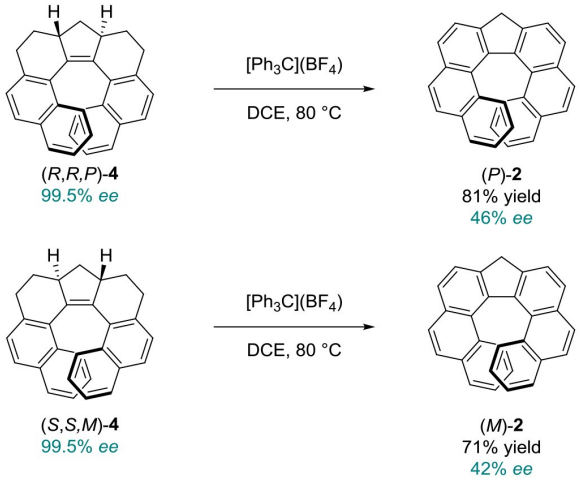

Scheme 4. Synthesis of enantioenriched Flu[7]helicene **2** form enantiopure partially hydrogenated helicenes **4**.

An obvious reason for this loss of enantiopurity would be a configurational instability of product **2** under the reaction conditions. As no data was available on this process, we decided to experimentally quantify the racemization for compound **2**. Thus, the kinetic of enantiomerization of (*P*)-**2** in chlorobenzene at 132 °C gave access to the experimental inversion barrier value of 142.3 kJ.mol^{-1}. While being a little bit smaller than the enantiomerization barrier for [6]-carbohelicene (151 kJ.mol^{-1}),[33] this barrier showed that fluoreno[7]helicene **2** is configurationally stable at 80 °C [$t_{1/2}$ > 2 years]. The loss of enantiopurity might be thus ascribed to a configurational instability of some intermediate generated during the reaction. A reasonable possibility would be the formation of a 1,3-cyclopentadiene as the central 5-membered ring by abstraction of a hydride at one of the stereogenic allylic positions by tritylium cation followed by loss of a proton on the apical methylene group. A suprafacial [1,5]-hydrogen shift would then readily occur on this intermediate leading to a scrambling of the remaining stereogenic center within the topical ring and to a loss of the chiral information.[34]

Conclusion

In this paper we have reported the synthesis of the new, partially hydrogenated fluoreno[*5*]-and [*7*]helicenes H_6-Flu[*n*]helicenes by a straightforward McMurry coupling as key cyclization step. The interplay between the central and helical chirality types has been established within these cyclic compounds. For each compound, the successful isomer separation and isolation of the two configurationally stable enantiomers (*R,R,P*) and (*S,S,M*), supplemented by quantum-chemical calculations, indicate that the helicity is induced by the configuration

of the two pre-formed stereogenic carbon atoms. Moreover, due to the presence of two rather-flexible cyclohexenyl rings, the helical configuration in the (*R,S,P*)/(*S,R,M*) couple is not stable at room temperature leading to the perception of this couple as the achiral, meso (*R,S*) compounds at that temperature. As typical helical compounds, the chiral (*R,R,P*) and (*S,S,M*) H_6-Flu[*n*]helicenes display clear, strong responses in VCD and ECD spectroscopy.

Finally, the H_6-Flu[*n*]helicenes constitute valuable intermediates to access on gram-quantities the corresponding aromatic fluoreno[*n*]helicenes through an oxidative dehydrogenation. The synthesis of helical NHC ligands by the combination of the latter fluoreno[*n*]helicenes with carbenic units is currently under study in our laboratories and will be reported in due course.

Acknowledgements

We thank the Centre National de la Recherche Scientifique (CNRS) and the University of Rennes. This work was supported by the Agence Nationale de la Recherche (ANR-16-CE07-0019 "Hel-NHC" grant). L.A. and J.A. acknowledge the Center for Computational Research (CCR) at the University at Buffalo for providing computational resources.[35] The computational part of this research has been supported by Grant CHE-1855470 from the National Science Foundation.

Conflict of Interest

The authors declare no conflict of interest.

Keywords: chiral resolution · chiroptics · fluorene · helicene · quantum-chemical calculations

[1] a) Y. Shen, C.-F. Chen, *Chem. Rev.* **2012**, *112*, 1463–1535; b) M. Gingras, *Chem. Soc. Rev.* **2013**, *42*, 1051–1095; c) M. Gingras, G. Felix, R. Peresutti, *Chem. Soc. Rev.* **2013**, *42*, 1007–1050; d) M. Gingras, *Chem. Soc. Rev.* **2013**, *42*, 968–1006; e) C.-F. Chen, Y. Shen, *Helicene Chemistry: From Synthesis to Applications*, Springer, Berlin, **2017**; f) M. Hasan, V. Borovkov, *Symmetry* **2018**, *10*, 10.

[2] W.-L. Zhao, M. Li, H.-Y. Lu, C.-F. Chen, *Chem. Commun.* **2019**, *55*, 13793–13803.

[3] Review: J. R. Brandt, F. Salerno, M. J. Fuchter, *Nat. Rev. Chem.* **2017**, *1*, 0045.

[4] Selected examples: a) F. Chen, W. Gu, A. Saeki, M. Melle-Franco, A. Mateo-Alonso, *Org. Lett.* **2020**, *22*, 3706–3711; b) P. Josse, L. Favereau, C. Shen, S. Dabos-Seignon, P. Blanchard, C. Cabanetos, J. Crassous, *Chem. Eur. J.* **2017**, *23*, 6277–6281; c) Y. Yang, R. C. da Costa, D.-M. Smilgies, A. J. Campbell, M. J. Fuchter, *Adv. Mater.* **2013**, *25*, 2624–2628.

[5] a) M. Roy, V. Berezhnaia, M. Villa, N. Vanthuyne, M. Giorgi, J.-V. Naubron, S. Poyer, V. Monnier, L. Charles, Y. Carissan, D. Hagebaum-Reignier, J. Rodriguez, M. Gingras, Y. Coquerel, *Angew. Chem. Int. Ed.* **2020**, *59*, 3264–3271; *Angew. Chem.* **2020**, *132*, 3290–3297; b) K. Nakano, H. Oyama, Y. Nishimura, S. Nakasako, K. Nozaki, *Angew. Chem. Int. Ed.* **2012**, *51*, 695–699; *Angew. Chem.* **2012**, *124*, 719–723; c) M. A. Shcherbina, X. Zeng, T. Tadjiev, G. Ungar, S. H. Eichhorn, K. E. S. Phillips, T. J. Katz, *Angew. Chem. Int. Ed.* **2009**, *48*, 7837–7840; *Angew. Chem.* **2009**, *121*, 7977–7980.

[6] a) H. Isla, N. Saleh, J.-K. Ou-Yang, K. Dhbaibi, M. Jean, M. Dziurka, L. Favereau, N. Vanthuyne, L. Toupet, B. Jamoussi, M. Srebro-Hooper, J. Crassous, *J. Org. Chem.* **2019**, *84*, 5383–5393; b) P. Ravat, T. Šolomek, M. Juríček, *ChemPhotoChem* **2019**, *3*, 180–186; c) H. Isla, J. Crassous, *C. R. Chim.* **2016**, *19*, 39–49.

[7] Selected reviews: a) L. W. Fang Lei, S. Yun, C. Chuanfeng, *Chin. J. Org. Chem.* **2018**, *38*, 541–554; b) P. Aillard, A. Voituriez, A. Marinetti, *Dalton Trans.* **2014**, *43*, 15263–15278.

[8] K. Dhbaibi, L. Favereau, J. Crassous, *Chem. Rev.* **2019**, *119*, 8846–8953.

[9] I. G. Stará, I. Starý, *Acc. Chem. Res.* **2020**, *53*, 144–158.

[10] a) J. Bosson, J. Gouin, J. Lacour, *Chem. Soc. Rev.* **2014**, *43*, 2824–2840; b) P. E. Reyes-Gutiérrez, M. Jirásek, L. Severa, P. Novotná, D. Koval, P. Sázelová, J. Vávra, A. Meyer, I. Císařová, D. Šaman, R. Pohl, P. Štěpánek, P. Slavíček, B. J. Coe, M. Hájek, V. Kašička, M. Urbanová, F. Teplý, *Chem. Commun.* **2015**, *51*, 1583–1586; c) R. Duwald, J. Bosson, S. Pascal, S. Grass, F. Zinna, C. Besnard, L. Di Bari, D. Jacquemin, J. Lacour, *Chem. Sci.* **2020**, *11*, 1165–1169 and references therein.

[11] Reviews: a) J. OuYang, J. Crassous, *Coord. Chem. Rev.* **2018**, *376*, 533–547; b) N. Saleh, C. Shen, J. Crassous, *Chem. Sci.* **2014**, *5*, 3680–3694.

[12] For helicene-NHCs, please see: a) E. S. Gauthier, L. Abella, N. Hellou, B. Darquié, E. Caytan, T. Roisnel, N. Vanthuyne, L. Favereau, M. Srebro-Hooper, J. A. G. Williams, J. Autschbach, J. Crassous, *Angew. Chem. Int. Ed.* **2020**, *59*, 8394–8400; *Angew. Chem.* **2020**, *132*, 8472–8478; b) M. Karras, M. Dąbrowski, R. Pohl, J. Rybáček, J. Vacek, L. Bednárová, K. Grela, I. Starý, I. G. Stará, B. Schmidt, *Chem. Eur. J.* **2018**, *24*, 10994–10998; c) I. G. Sanchez, M. Samal, J. Nejedly, M. Karras, J. Klivar, J. Rybacek, M. Budesinsky, L. Bednarova, B. Seidlerova, I. G. Stara, I. Stary, *Chem. Commun.* **2017**, *53*, 4370–4373; d) N. Hellou, M. Srebro-Hooper, L. Favereau, F. Zinna, E. Caytan, L. Toupet, V. Dorcet, M. Jean, N. Vanthuyne, J. A. G. Williams, L. Di Bari, J. Autschbach, J. Crassous, *Angew. Chem. Int. Ed.* **2017**, *56*, 8236–8239; *Angew. Chem.* **2017**, *129*, 8348–8351; e) N. Hellou, C. Jahier-Diallo, O. Basle, M. Srebro-Hooper, L. Toupet, T. Roisnel, E. Caytan, C. Roussel, N. Vanthuyne, J. Autschbach, M. Mauduit, J. Crassous, *Chem. Commun.* **2016**, *52*, 9243–9246.

[13] L. Pallova, PhD thesis, Toulouse III University, Paul Sabatier, **2020**.

[14] Selected references: a) F. Pammer, Y. Sun, W. R. Thiel, *Inorg. Chim. Acta* **2011**, *374*, 205–210; b) F. Pammer, Y. Sun, D. Weismann, H. Sitzmann, W. R. Thiel, *Chem. Eur. J.* **2010**, *16*, 1265–1270; c) F. Pammer, Y. Sun, M. Sieger, J. Fiedler, B. Sarkar, W. R. Thiel, *Organometallics* **2010**, *29*, 6165–6168; d) F. Pammer, Y. Sun, W. R. Thiel, *Organometallics* **2008**, *27*, 1015–1018; e) F. Pammer, Y. Sun, M. Pagels, D. Weismann, H. Sitzmann, W. R. Thiel, *Angew. Chem. Int. Ed.* **2008**, *47*, 3271–3274; *Angew. Chem.* **2008**, *120*, 3315–3318; f) F. Pammer, Y. Sun, C. May, G. Wolmershäuser, H. Kelm, H.-J. Krüger, W. R. Thiel, *Angew. Chem. Int. Ed.* **2007**, *46*, 1270–1273; *Angew. Chem.* **2007**, *119*, 1293–1296; g) R. H. Martin, *J. Chem. Soc.* **1941**, 679–685.

[15] a) H. Oyama, M. Akiyama, K. Nakano, M. Naito, K. Nobusawa, K. Nozaki, *Org. Lett.* **2016**, *18*, 3654–3657; b) M. Akiyama, K. Nozaki, *Angew. Chem. Int. Ed.* **2017**, *56*, 2040–2044; *Angew. Chem.* **2017**, *129*, 2072–2076; c) M. Akiyama, Y. Tsuchiya, A. Ishii, M. Hasegawa, Y. Kurashige, K. Nozaki, *Chem. Asian J.* **2018**, *13*, 1902–1905.

[16] See also: Y. Sawada, S. Furumi, A. Takai, M. Takeuchi, K. Noguchi, K. Tanaka, *J. Am. Chem. Soc.* **2012**, *134*, 4080–4083.

[17] a) N. Koumura, R. W. J. Zijlstra, R. A. van Delden, N. Harada, B. L. Feringa, *Nature* **1999**, *401*, 152–155; b) N. Harada, N. Koumura, B. L. Feringa, *J. Am. Chem. Soc.* **1997**, *119*, 7256–7264.

[18] a) B. L. Feringa, *Angew. Chem. Int. Ed.* **2017**, *56*, 11060–11078; *Angew. Chem.* **2017**, *129*, 11206–11226; b) B. L. Feringa, *Acc. Chem. Res.* **2001**, *34*, 504–513.

[19] a) F. H. V. Chau, E. J. Corey, *Tetrahedron Lett.* **2006**, *47*, 2581–2583; b) T. Mackewitz, M. Roeper, EP patent 1036796, **2000**.

[20] See the Supporting Information for details.

[21] M. J. Frisch, G. W. Trucks, H. B. Schlegel et al., "Gaussian 16, Revision B.01", Gaussian, Inc., Wallingford CT, **2016**. URL: www.gaussian.com.

[22] A. D. Becke, *J. Chem. Phys.* **1993**, *98*, 5648–5652.

[23] a) F. Weigend, R. Ahlrichs, *Phys. Chem. Chem. Phys.* **2005**, *7*, 3297–3305; b) F. Weigend, *Phys. Chem. Chem. Phys.* **2006**, *8*, 1057–1065.

[24] G. Scalmani, M. J. Frisch, *J. Chem. Phys.* **2010**, *132*, 114110.

[25] Deposition Numbers 2055562 ((*R,R,P*)-**4**) and 2054763 ((*R,S*)-**4**) contain the supplementary crystallographic data for this paper. These data are provided free of charge by the joint Cambridge Crystallographic Data Centre and Fachinformationszentrum Karlsruhe Access Structures service www.ccdc.cam.ac.uk/structures.

[26] F. H. Allen, O. Kennard, D. G. Watson, L. Brammer, A. G. Orpen, R. Taylor, *J. Chem. Soc. Perkin Trans. 2* **1987**, *0*, S1–S19.

[27] M. K. J. ter Wiel, R. A. van Delden, A. Meetsma, B. L. Feringa, *J. Am. Chem. Soc.* **2003**, *125*, 15076–15086.

[28] a) W. H. Laarhoven, W. J. C. Prinsen, *Top. Curr. Chem.* **1984**, *125*, 63–130; b) Y. Yoshida, Y. Nakamura, H. Kishida, H. Hayama, Y. Nakano, H. Yamochi, G. Saito, *CrystEngComm* **2017**, *19*, 3626–3632.
[29] a) L. A. Nafie, *Vibrational Optical Activity: Principles and Applications*, Wiley-VCH, New York, **2011**; b) L. D. Barron, *Molecular Light Scattering and Optical Activity*, 2nd ed., Cambridge University Press, Cambridge, **2004**.
[30] Selected examples: a) S. Abbate, G. Longhi, F. Lebon, E. Castiglioni, S. Superchi, L. Pisani, F. Fontana, F. Torricelli, T. Caronna, C. Villani, R. Sabia, M. Tommasini, A. Lucotti, D. Mendola, A. Mele, D. A. Lightner, *J. Phys. Chem. C* **2014**, *118*, 1682–1695; b) A. Bensalah-Ledoux, D. Pitrat, T. Reynaldo, M. Srebro-Hooper, B. Moore, II, J. Autschbach, J. Crassous, S. Guy, L. Guy, *Chem. Eur. J.* **2016**, *22*, 3333–3346; c) C. Shen, M. Srebro-Hooper, T. Weymuth, F. Krausbeck, J. T. López Navarrete, F. J. Ramírez, B. Nieto-Ortega, J. Casado, M. Reiher, J. Autschbach, J. Crassous, *Chem. Eur. J.* **2018**, *24*, 15067–15079.
[31] a) C. Adamo, V. Barone, *J. Chem. Phys.* **1999**, *110*, 6158–6169; b) M. Ernzerhof, G. E. Scuseria, *J. Chem. Phys.* **1999**, *110*, 5029–5036.
[32] a) M. Srebro-Hooper, J. Autschbach, *Annu. Rev. Phys. Chem.* **2017**, *68*, 399–420; b) J. Autschbach, L. Nitsch-Velasquez, M. Rudolph, *Top. Curr. Chem.* **2011**, *298*, 1–98.
[33] R. H. Martin, M. J. Marchant, *Tetrahedron Lett.* **1972**, *13*, 3707–3708.
[34] a) B. A. Hess, J. E. Baldwin, *J. Org. Chem.* **2002**, *67*, 6025–6033; b) W. R. Roth, *Tetrahedron Lett.* **1964**, *5*, 1009–1013.
[35] Center for Computational Research, University at Buffalo, http://www.buffalo.edu/ccr.html.

Manuscript received: January 14, 2021
Accepted manuscript online: March 29, 2021
Version of record online: ■■, ■■■

FULL PAPER

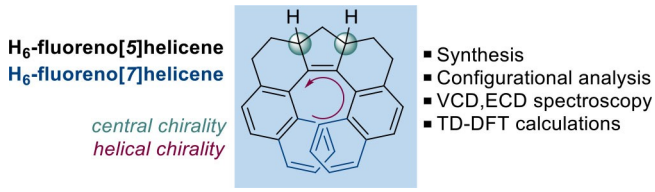

Blocking a molecular motor: The partially saturated H_6-fluoreno[*n*]helicenes (see figure), cyclic analogs of the well-known Feringa's molecular motors, are produced via a similar McMurry cyclization approach. While being composed of three diastereoisomers, they serve as valuable intermediates for the efficient, multigram scale access to the aromatic fluoreno[*n*]helicenes.

Dr. L. Pallova, Dr. E. S. Gauthier, Dr. L. Abella, M. Jean, Dr. N. Vanthuyne, Dr. V. Dorcet, Dr. L. Vendier, Prof. J. Autschbach, Dr. J. Crassous*, Dr. S. Bastin*, Dr. V. César**